



Universiteit
Leiden
The Netherlands

Automated quantification of the pulmonary vasculature in pulmonary embolism and chronic thromboembolic pulmonary hypertension

Zhai, Z.W.; Boon, G.J.A.M.; Staring, M.; Dam, L.F. van; Kroft, L.J.M.; Girón, I.H.; ... ; Stoel, B.C.

Citation

Zhai, Z. W., Boon, G. J. A. M., Staring, M., Dam, L. F. van, Kroft, L. J. M., Girón, I. H., ... Stoel, B. C. (2023). Automated quantification of the pulmonary vasculature in pulmonary embolism and chronic thromboembolic pulmonary hypertension. *Pulmonary Circulation*, 13(2). doi:10.1002/pul2.12223


Version: Publisher's Version

License: [Creative Commons CC BY-NC 4.0 license](https://creativecommons.org/licenses/by-nc/4.0/)

Downloaded from: <https://hdl.handle.net/1887/3714206>

Note: To cite this publication please use the final published version (if applicable).

Automated quantification of the pulmonary vasculature in pulmonary embolism and chronic thromboembolic pulmonary hypertension

Zhiwei Zhai¹  | Gudula J. A. M. Boon² | Marius Staring¹ |
 Lisette F. van Dam² | Lucia J. M. Kroft³ | Irene Hernández Girón¹ |
 Maarten K. Ninaber⁴ | Harm Jan Bogaard⁵ | Lilian J. Meijboom⁶ |
 Anton Vonk Noordegraaf⁵ | Menno V. Huisman² | Frederikus A. Klok² |
 Berend C. Stoel¹

¹Division of Image Processing, Department of Radiology, Leiden University Medical Center, Leiden, The Netherlands

²Department of Medicine - Thrombosis and Hemostasis, Leiden University Medical Center, Leiden, The Netherlands

³Department of Radiology, Leiden University Medical Center, Leiden, The Netherlands

⁴Department of Pulmonology, Leiden University Medical Center, Leiden, The Netherlands

⁵Department of Pulmonary Medicine, Amsterdam Cardiovascular Sciences, Amsterdam UMC, Vrije Universiteit Amsterdam, Amsterdam, The Netherlands

⁶Department of Radiology and Nuclear Medicine, Amsterdam UMC, Vrije Universiteit Amsterdam, Amsterdam, The Netherlands

Correspondence

Berend C. Stoel, Division of Image Processing, Department of Radiology, Leiden University Medical Center, Albinusdreef 2, 2300RC, Leiden, The Netherlands.
 Email: b.c.stoel@lumc.nl

Abstract

The shape and distribution of vascular lesions in pulmonary embolism (PE) and chronic thromboembolic pulmonary hypertension (CTEPH) are different. We investigated whether automated quantification of pulmonary vascular morphology and densitometry in arteries and veins imaged by computed tomographic pulmonary angiography (CTPA) could distinguish PE from CTEPH. We analyzed CTPA images from a cohort of 16 PE patients, 6 CTEPH patients, and 15 controls. Pulmonary vessels were extracted with a graph-cut method, and separated into arteries and veins using deep-learning classification. Vascular morphology was quantified by the slope (α) and intercept (β) of the vessel radii distribution. To quantify lung perfusion defects, the median pulmonary vascular density was calculated. By combining these measurements with densities measured in parenchymal areas, pulmonary trunk, and descending aorta, a static perfusion curve was constructed. All separate quantifications were compared between the three groups. No vascular morphology differences were detected in contrast to vascular density values. The median vascular density (interquartile range) was -567 (113), -452 (95), and -470 (323) HU, for the control, PE, and CTEPH group. The static perfusion curves showed different patterns between groups, with a statistically significant difference in aorta-pulmonary trunk gradient between the PE and CTEPH groups ($p = 0.008$). In this proof of concept study, not vasculature morphology but densities differentiated between patients of three groups. Further technical improvements are needed to allow for accurate differentiation between PE and CTEPH, which in this study was only possible

This is an open access article under the terms of the Creative Commons Attribution-NonCommercial License, which permits use, distribution and reproduction in any medium, provided the original work is properly cited and is not used for commercial purposes.

© 2023 The Authors. *Pulmonary Circulation* published by John Wiley & Sons Ltd on behalf of Pulmonary Vascular Research Institute.

Funding information

Hartstichting, Grant/Award Number: 2017T064; Merck Sharp and Dohme

statistically by measuring the density gradient between aorta and pulmonary trunk.

KEYWORDS

CTEPH, CTPA, pulmonary, pulmonary embolism, vessel

INTRODUCTION

Chronic thromboembolic pulmonary hypertension (CTEPH) is a rare but severe long-term complication of acute pulmonary embolism (PE), which is caused by persistent obstruction of pulmonary arteries and vascular remodeling.^{1–4} Diagnosing CTEPH is challenging with reported diagnostic delays ranging between 1 and 2 years, and these delays are associated with higher mortality.^{3,5–8}

Different studies have shown that computed tomographic pulmonary angiography (CTPA) performed to diagnose PE often already shows clear signs of CTEPH.^{3,9–13} Since these CTPA images are assessed visually, reproducibility and sensitivity of these assessments are limited in clinical practice circumstances, where often CTEPH expert radiologists are not available, and signs of CTEPH usually remain undetected.^{14,15} Algorithms based on Artificial Intelligence (AI) may be able to facilitate and improve these assessments of chronicity, allowing for early detection of CTEPH. Currently, however, such algorithms are not available.

We performed a proof of concept study to test whether automated quantification of pulmonary vascular morphology and densitometry could be helpful in differentiating between acute PE and CTEPH. To do so, we quantified pulmonary vascular remodeling and static vascular perfusion by post-processing of CTPA images in a group of PE and CTEPH patients and in a control group of patients suspected of pulmonary embolism but with normal CT scans. With the recent advances of AI-based techniques in automatically distinguishing pulmonary arteries and veins, we studied whether the quantification of remodeling and static perfusion can be made more specific.

MATERIALS AND METHODS**Patients**

We studied clinical CTPA scans from a convenience cohort of 37 patients from the Leiden University Medical Center, including 16 patients with acute PE, 6 patients with CTEPH, proven by pulmonary angiography and

right heart catheterization (RHC), and a control group of 15 cases, in whom PE was suspected but ruled out by CTPA, and in whom no radiological signs of CTEPH were detected. Patients were selected from previous studies based on the availability of the CTPA images, the use of the same CT scanner (within each group), and the completeness of follow-up.^{16–20} The local Medical Ethical Committee had approved the study protocols and patients provided informed consent for participation in the original studies. The current post-hoc study was approved by the local Medical Ethical Committee which waived the need for new informed consent due to the observational study design.

In all PE patients, CTEPH was ruled out by echocardiography after a 2-year follow-up, and none of the control patients was diagnosed with either PE or CTEPH during the 2-year follow-up.

CTPA analysis

The PE patients and controls were scanned with an Aquilion 64 scanner (Canon Medical System); in half-inspiration to avoid Valsalva maneuvers. Patients in the CTEPH group were scanned with an Aquilion ONE scanner (Canon Medical System), in half-inspiration. CT settings were as follows: 100–120 kVp, automatic tube current modulation; 40 × 0.5 mm and 64 × 0.5 mm collimation; images were reconstructed using an FC12, FC07, or FC08 kernel, with a slice thickness of 1.0 mm and an increment of 0.5 mm. Contrast enhancement was performed on the Aquilion 64 scanner using a bolus triggered from the pulmonary trunk, with 70 mL of sonicated Iopromid (Ultravist 370, Bayer Schering Pharma) at 5.0 mL/s, with 50 ml (5.0 mL/s) saline flushing, for typical body weights between 65 and 80 kg. For the Aquilion ONE scanner, these boli were 75 mL (4.5 mL/s) and 45 ml (4.5 mL/s), respectively.

First, lung volumes were extracted from the CTPA scans using a multi-atlas segmentation method. Within the lung volumes, pulmonary vessels were segmented with a graph-cut method, where shape features and CT intensities of vessels were combined into a single cost function.²¹ The extracted pulmonary vessels were then classified into arteries and veins by a deep learning (DL) model.²² In this

classification method, a vessel graph was first constructed based on the skeletonization of the extracted vessels. Subsequently, the DL model was applied, which combines a convolutional neural network and a graph convolutional network, to classify the graph nodes into either pulmonary arteries or veins. Pulmonary artery and vein volumes were constructed based on the graph node classification (see Figure 1).

To quantify the vascular morphology, a radius histogram was calculated by counting the occurrence of vessel radii, and a linear regression was performed on the radius histogram.²¹ Subsequently, the vascular slope α and intercept β of the regression line were calculated. Slope α then indicates pruning of small vessels and/or dilation of larger vessels. Intercept β is an extrapolation of the radius histogram to radius 0, which relates to the capacity of the vascular tree. These morphologic quantifications were performed for all pulmonary vessels together and for arteries and veins separately.

To quantify perfusion defects, the densities (CT intensity values) of specific areas in the vasculature and parenchyma were quantified, following the order of the trajectory of blood flow through the lungs: starting at the pulmonary trunk, then measuring in the pulmonary arteries from large to small caliber, subsequently measuring in the parenchymal area, followed by the pulmonary venous tree (from small to large caliber), and finally measuring the density in the descending aorta (see Figure 2). For measuring blood densities within the pulmonary trunk and aorta, samples within a circular region of interest were taken automatically from the lumen, by iteratively increasing the radius until the standard error of the measurement reaches a minimum, to yield the most accurate sample.²³ For quantifying the perfusion defects in the vascular trees, the median density was determined of the vessel centerlines. Parenchyma static perfusion was assessed by the median density of the parenchymal area, defined as the collection

of voxels in the lungs that are located most distally to the vascular trees.²⁴ Static perfusion at different caliber levels within the arterial and venous trees were subdivided into quartiles (on a patient level), according to the local radius. The median density values were subsequently calculated for each quartile separately.

As global measures of static perfusion, the gradient in density between aorta and pulmonary trunk was calculated (i.e., the above-mentioned aortic density minus pulmonary trunk density), and the median of the vascular densities was calculated for all pulmonary vessels together and for arteries and veins, separately.

Finally, lung volume and voxel size were recorded as possible confounding factors since density measurements could be influenced by lung size,²⁵ and the vascular imaging biomarkers may be affected by voxel size,²⁶ which in turn is related to patient size (due to the fixed reconstruction matrix in CT). As body mass could have an influence on the image quality and therefore produce false positive detection of pulmonary vessels, body mass index (BMI) was also considered a possible confounder.

Statistical analysis

All statistical analyses were performed by using SPSS (Version 23.0.0; IBM Corp.). A two-tailed p -value below 0.05 was considered statistically significant. For the patient characteristics, continuous variables are presented as mean and standard deviation (SD), and categorical variables are presented as frequencies and percentages.

To investigate possible confounding effects of lung volume, voxel size, and BMI, their correlations with all lung imaging biomarkers were tested. If a significant (Spearman) correlation was found (after correcting for multiple testing), lung volume, voxel size, or BMI were

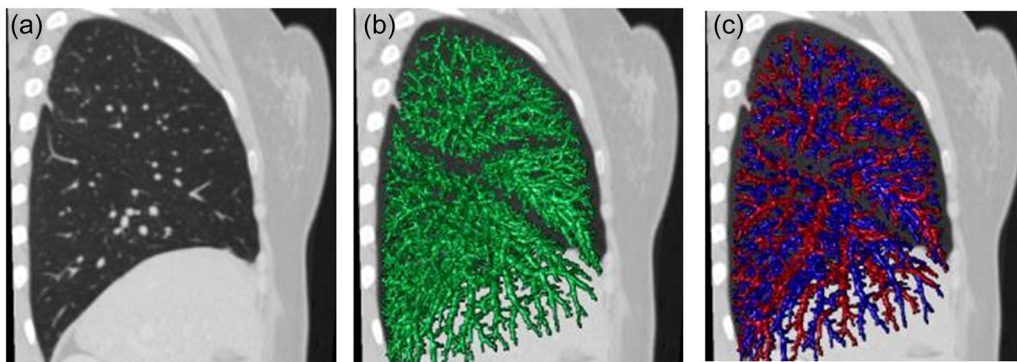


FIGURE 1 Illustration of deep learning-based artery-vein separation (a) sagittal view of the right lung in a chest computed tomography; (b) extracted vessels; (c) classified pulmonary arteries and veins, in blue and red, respectively.

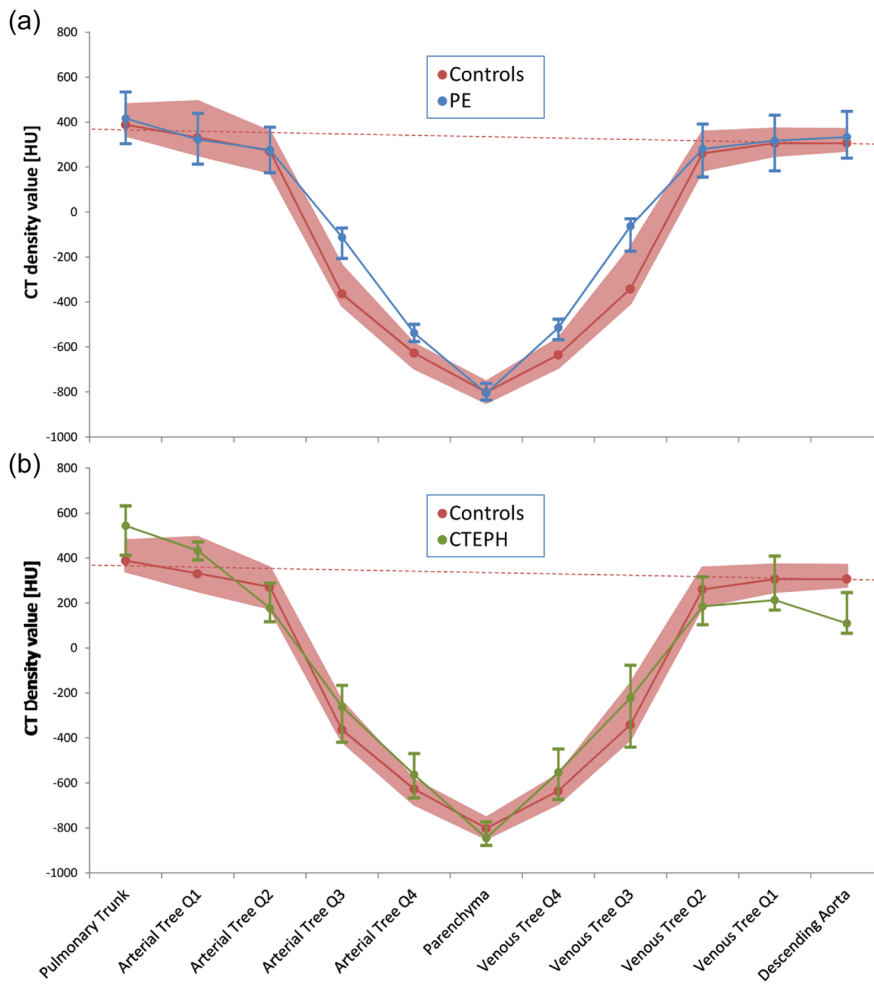


FIGURE 2 Different static perfusion patterns. Density values for the arterial and venous trees were subdivided in four quartiles according to their caliber, where the 1st quartile (Q1) represents the larger (proximal) vessels, and the 4th quartile (Q4), the smallest (distal) vessels. The error bars indicate the median values and inter-quartile range. For controls, the interquartile range is indicated by the red area. The red dashed line indicates the approximate shape of the curve, without imaging artifacts (i.e., partial volume effects and reconstruction errors). (a) Controls versus PE: the PE group has higher density values in the smaller arteries and veins (Q3 and Q4), producing a V-shape. (b) Controls versus CTEPH: in CTEPH the smallest vessels (Q3 and Q4) have also higher densities than controls. Additionally, densities are higher in the pulmonary trunk and lower in the descending aorta, producing a tilted V-shape.

TABLE 1 Patient characteristics of the groups of PE, controls, and CTEPH.

Characteristic	PE (n = 16)	Control (n = 15)	CTEPH (n = 6)	p-value
Gender (M/F)	7/9	6/9	3/3	0.915
Mean age (SD) [years]	56.8 (12.6)	51.7 (17.2)	68.8 (7.2)	0.032*
Mean length (SD) [m]	1.75 (0.07)	1.74 (0.07)	1.73 (0.09)	0.726
Mean weight (SD) [kg]	93.9 (16.5)	79.9 (16.4)	71.1 (12.9)	0.009*
Mean BMI (SD)	30.4 (4.48)	26.4 (4.88)	23.6 (2.98)	0.004*
Mean CT lung volume (SD) [L]	3.42 (0.84)	4.00 (1.10)	5.13 (1.96)	0.076

Abbreviations: BMI, body mass index; CTEPH, chronic thromboembolic pulmonary hypertension; PE, pulmonary embolism; SD, standard deviation.

*p-value < 0.05 (Kruskal–Wallis test).

considered covariates in testing the differences between groups. Therefore, a nonparametric analysis of covariance (Quade's ANCOVA) was performed to analyze the imaging biomarkers with lung volume, voxel size, or BMI as co-variates in differentiating between the three groups; PE, CTEPH, and control. To ensure such corrections would be effective, these ANCOVA tests were only performed after confirmation that the covariates did not differ between patient groups. If no covariates were

required, a Kruskal–Wallis test was applied to determine the significance of the differences between groups.

RESULTS

Patient characteristics are shown in Table 1. There were differences between groups in terms of age, weight, and BMI, where the CTEPH patients were, on average older

than the PE group and the controls. The mean BMI was highest in the PE group.

From the confounder analysis, it was confirmed that voxel size influences the morphology biomarker α for the total vascular and arterial tree ($R=0.43$ and 0.46 , respectively), but not for the venous tree ($R=0.14$, $p=0.42$). All vascular density measurements were correlated with lung volume (R ranging from -0.46 to -0.63). This correlation with volume was also found for biomarker α for the total vascular tree ($R=0.33$). As none of the required covariates differed between patient groups, we performed a non-parametric ANCOVA, with voxel size as a covariate for the slope parameters α , and with lung volume as a covariate for the vascular density measurements.

The morphology and density measurements of each patient group are presented in Table 2. The morphology biomarkers, α and β , did not differ between the patient groups. Only numerically, there was a trend that the vascular intercept β indicated a difference in median capacity between groups ($p=0.069$), with the lowest capacity in the CTEPH group ($9.9 \log(\mu\text{L})$) as compared to the controls ($11.2 \log(\mu\text{L})$) and to PE patients ($10.9 \log(\mu\text{L})$). To compare with other previously published parameters on vessel morphology,²⁷ the ratio of

small-vessel volume (blood volume of vessels with a cross-sectional area of $\leq 5 \text{ mm}^2$, BV5) and total blood vessel volume (TBV) and the ratio of large-vessel volume (a cross-sectional area of $>10 \text{ mm}^2$, BV > 10) and TBV are also shown in Table 2, but did not differ between groups either.

The density biomarkers, however, did differ between the three groups, where less contrast media (lower HU values) remained in the pulmonary vascular tree in the controls, as compared to both PE and CTEPH. The gradient in blood density between aorta and pulmonary trunk was also different between groups, where the median gradient was smallest in the control group (-68 HU), as compared to PE (-94 HU) and CTEPH (-343 HU). In the post hoc analysis, the difference in aorta-pulmonary trunk gradient was found to be statistically significant between the PE and CTEPH groups ($p=0.008$).

In Figure 2, all local density measurements are plotted for the three patient groups, following the flow of contrast medium from the pulmonary trunk into the proximal arteries (1st quartile) to the more distal arteries (4th quartile) through the parenchymal areas, into the distal veins (4th quartile) through the proximal veins (1st quartile), and finally after passing the left side of the heart into the descending aorta. The curve of the controls

TABLE 2 Comparison of pulmonary vasculature quantifications between PE, controls, and CTEPH.

Parameter	PE (n = 16)	Control (n = 15)	CTEPH (n = 6)	p-value
Vascular slope (α) ^a	-1.9 (0.3)	-2.0 (0.4)	-1.3 (0.9)	0.148 ^a
Vascular intercept (β) ^b	10.9 (0.6)	11.2 (0.7)	9.9 (1.8)	0.069 ^b
Arterial slope (α) ^a	-1.8 (0.2)	-1.9 (0.3)	-1.8 (0.7)	0.931 ^a
Arterial intercept (β) ^b	10.4 (0.6)	10.5 (0.8)	10.3 (1.5)	0.790 ^b
Venous slope (α) ^b	-2.0 (0.2)	-2.1 (0.4)	-1.9 (0.4)	0.488 ^b
Venous intercept (β) ^b	9.8 (0.4)	9.8 (0.6)	9.5 (1.1)	0.785 ^b
Small vessel ratio (BV5/TBV) ^a	0.38 (0.06)	0.41 (0.13)	0.46 (0.11)	0.203 ^a
Large vessel ratio (BV > 10/TBV) ^a	0.41 (0.10)	0.36 (0.11)	0.34 (0.14)	0.116 ^a
Parenchymal density ^c	-806 (82)	-802 (99)	-845 (149)	0.787 ^c
Vascular density ^c	-452 (95) ¹	-567 (113)	-470 (323) ²	0.006 ^c
Arterial density ^c	-466 (95) ³	-564 (113)	-481 (311) ⁴	0.008 ^c
Venous density ^c	-427 (109) ⁵	-576 (130)	-446 (352) ⁶	0.014 ^c
Aorta-pulmonary trunk gradient ^b	-94 (167) ^{7†}	-68 (66)	-343 (258) ^{8†}	0.015 ^b

Note: Median values (interquartile range). Slopes, α , are expressed in $\text{mm}/\log(\mu\text{L})$ and intercepts, β , in $\log(\mu\text{L})$. Density values are presented in Hounsfield Units (HU). Post hoc analysis: ^{1,3,5,7}PE vs. controls, p -values: 0.015, 0.019, 0.033, and 0.545, respectively; ^{2,4,6,8}CTEPH vs. controls, p -values: 0.048, 0.054, 0.066, and 0.008, respectively. [†]Post hoc test, CTEPH vs. PE: p -value = 0.008.

Abbreviations: ANCOVA, analysis of covariance; BV5, blood volume of vessels with a cross-sectional area of $\leq 5 \text{ mm}^2$; BV > 10 : blood volume of vessels with a cross-sectional area of $>10 \text{ mm}^2$; CTEPH, chronic thromboembolic pulmonary hypertension; PE, pulmonary embolism; TBV, total blood vessel volume.

^aNonparametric ANCOVA, corrected for voxel size.

^bKruskal-Wallis test.

^cNonparametric ANCOVA, corrected for lung volume.

forms a U-shape, whereas both PE and CTEPH form more of a V-shape, indicating that most of the differences occur in the vessels with diameters in the 3rd and 4th quartile (for arteries: $p = 0.009$ and 0.012 , respectively; and for veins: $p = 0.032$ and 0.014 , respectively). For the CTEPH group, the V-shape is asymmetric, as compared to the PE group, indicating that more contrast media has remained in the pulmonary trunk and less contrast media has reached the larger veins and aorta (the green curve in Figure 2 is on the left side higher than the controls, but lower on the right side). This asymmetry is confirmed by the difference found in the aorta-pulmonary trunk gradient between PE and CTEPH (Mann-Whitney U test, $p = 0.006$). The dashed line in Figure 2 in the control curve indicates how the curve theoretically should look without image acquisition artifacts.

DISCUSSION

We studied the pulmonary vasculature in patients with PE and CTEPH and compared these results to a control group without obstructive pulmonary artery disease. Based on the CTPA scans, the pulmonary vascular morphology and perfusion defects were quantified by an automatic method for all pulmonary vessels together and for arteries and veins separately, using deep learning. The morphology biomarkers, α and β , did not differ between patient groups, indicating that no PE- or CTEPH-specific vascular remodeling could be detected using the current technology of image acquisition and postprocessing. However, static perfusion measurements did differ between groups, with lower contrast concentrations in the control group, as compared to both patients with PE and CTEPH. The PE and CTEPH group differed significantly only in terms of the gradient between the aorta and pulmonary trunk. The contrast enhancement curves over the trajectory of blood flow (Figure 2) showed that contrast concentrations drop earlier and stay lower in controls (U-shape), as compared with both PE and CTEPH (V-shapes). This indicates that in obstructive pulmonary artery disease, contrast concentrations remain high in the central vessels and may reflect diffusely increased resistance in the pulmonary vasculature despite the localized obstruction. In the CTEPH group, the difference in contrast enhancement between the aorta and pulmonary trunk is higher than in PE, which is also illustrated in Figure 2 by the tilted V-curve in CTEPH. These findings of our proof-of-concept study may be useful in developing algorithms that differentiate between PE and CTEPH as well as help understanding the impact of PE and CTEPH on the pulmonary vasculature.

In previous publications, methods have been studied for estimating the impact of PE or CTEPH on pulmonary vascular morphology. In particular, one study²⁷ investigated the morphology in 18 CTEPH and 15 control patients. The ratio of small-vessel volume (blood volume of vessels with a cross-sectional area of $\leq 5 \text{ mm}^2$, BV5) and total blood vessel volume (TBV) was calculated as a proxy for small vessel pruning, and the ratio of large-vessel volume (a cross-sectional area of $>10 \text{ mm}^2$, BV > 10) and TBV was quantified as a proxy for large-vessel dilation. The quantifications of BV5/TBV and BV > 10 /TBV were different between CTEPH and control patients, implying that pulmonary vascular morphology was remodeled by CTEPH. In our current study, however, we were not able to reproduce these results. Possible explanations could be the differences in patient groups, but also differences in CT acquisition protocols, including contrast administration timing that may influence vessel detection, and differences in vessel segmentation and quantification methods.

Previously we investigated the perfusion in pulmonary vessels for CTEPH patients treated with balloon pulmonary angioplasty and quantified the perfusion changes by automatically comparing the CTPA scans of pre- and posttreatment.²⁴ This study showed that the perfusion changes in CTPA before and after treatment are correlated with the treatment effects in terms of hemodynamic changes measured with a right-sided heart catheterization. Therefore, this type of measurement based on CTPA may not only distinguish different patient groups, as suggested in this pilot study but is also able to detect perfusion changes over time for quantification of progression and treatment effects. In these types of follow-up studies, specifying perfusion changes for arteries and veins separately may also provide additional and more detailed information.

There are some limitations linked to the fact that this was a retrospective study. As a consequence, CT protocols had not been standardized, and we used two different scanners, not randomly distributed over the patient groups. Another source of variation could be the timing of the contrast enhancement, which may also introduce confounding. By measuring the relative difference between the input and output concentrations in the pulmonary trunk and aorta, we have tried to minimize this effect, which was confirmed in a post-hoc analysis, where no correlation was found between the Aorta-Pulmonary trunk gradient and the delay time between contrast administration and CT scanning (Figure 3). Differences in contrast volume and flow rate remain possible confounders. Another limitation is that we could not adjust our algorithm for cardiac output and function as well as total thrombus load. Additionally, the

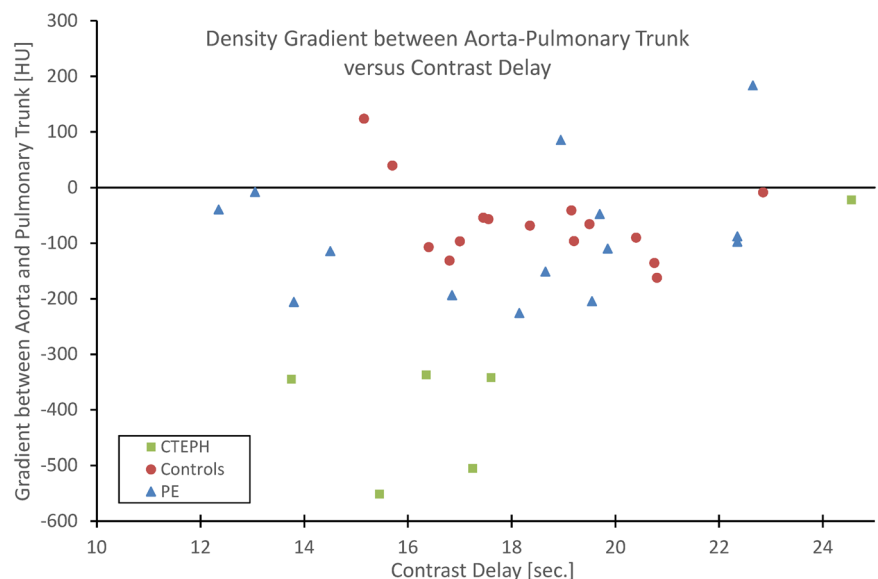
difference in age between patient groups could also have played a role in producing the differences found in this study, as lung perfusion generally decreases with age. Another limitation has been illustrated in Figure 2, where a U- and V-shape is presented in density measurements over the trajectory from pulmonary trunk to the descending aorta. The dotted line in this figure indicates the expected decay in density values. Certainly, negative HU values would not be expected, as this would indicate densities lower than water. Clearly, this artificial decrease in density values is caused by the so-called partial volume effect, where a voxel contains both vascular structures and air from bronchi/bronchioles. This effect is most prominent where the size of vessels reaches the limits of the resolution of CT. The fact that this effect is also seen in larger vessels (on the shoulder of the V and U shape) means that there are additional causes to this decay, probably from the image reconstruction methods, that are mostly optimized for human interpretation instead of quantification. In future work, we, therefore, aim to perform phantom analyses to study the effect of these differences on quantification and develop ways to determine the optimal CT settings, and develop correction methods to eliminate residual errors. Nonetheless, the difference in perfusion patterns between patient groups found in this study would likely remain after correction for these artifacts, since these effects are independent of the patient group. In this study, only a small group of 37 cases were investigated, therefore, validation in a much larger patient population is needed.

As far as image processing is concerned, there are nonetheless some limitations that affect the results of this study. Although we could make a distinction between

arteries and veins using deep learning methods with an accuracy of 74% in a subset of 10 CT scans of the current study group,²² there is still room for improvement for these deep learning methods. This subset of 10 CT scans consisted of three PE, five controls, and two CTEPH patients, in which the artery-vein separation was most successful in the controls (81%), whereas in PE and CTEPH patients, this accuracy was lower (71% and 68%, respectively). Therefore, especially in the target population, improvements are needed. One of the main hurdles to overcome is the manual generation of reference classifications, which takes disproportionately amount of time and effort, as this is the very reason for attempting to automate this task. Further improvements in vessel detection would benefit the ultimate accuracy, especially in filtering false positive detections due to severe lesions in the lung, such as consolidations and fibrotic tissue. Investigating the lung vessels in isolated regions, such as lobes, regions of large/small vessels, or affected/unaffected regions, would be a future research topic to make the quantifications more specific and sensitive to small changes. The perfusion measurements may then distinguish more accurately between patient groups.

We used the term static perfusion to indicate that the CT imaging protocol is not dynamic. This means that the quantified density values reflect the concentration of the contrast agent at only a one-time point. Therefore the quantification is more focused on perfusion detects than on perfusion itself. Dynamic perfusion measurements by Dynamic Contrast Enhance CT (DCE-CT) would probably further increase accuracy and independence on contrast administration timing, but current CT scanners cannot cover the entire lungs in one rotation, and to date, contrast and X-ray dosage prevent its use in daily practice.

FIGURE 3 Scatter plot of the density gradient between aorta and pulmonary trunk against the time delay between contrast injection and computed tomography scanning.



In this proof of concept study, not vasculature morphology but vascular densities differentiated between normal and thrombotic obstructed vasculature. Further technical improvements are needed to allow for accurate differentiation between PE and CTEPH, which was only possible at a group level with the gradient in blood density between the aorta and pulmonary trunk as an imaging biomarker.

ACKNOWLEDGMENTS

This study was supported by an unrestricted grant from Merck Sharp & Dohme (MSD). F.A. Klok and Gudula J.A.M. Boon were supported by the Dutch Heart Foundation (2017T064).

CONFLICTS OF INTEREST STATEMENT

The authors declare no conflicts of interest.

ETHICS STATEMENT

This study was performed in accordance with the Helsinki Declaration of 1975, as revised in 2008.

ORCID

Zhiwei Zhai  <http://orcid.org/0000-0002-4016-6000>

REFERENCES

- Kim NH, Delcroix M, Jais X, Madani MM, Matsubara H, Mayer E, Ogo T, Tapson VF, Ghofrani HA, Jenkins DP. Chronic thromboembolic pulmonary hypertension. *Eur Respir J*. 2019;53:1801915.
- Ende-Verhaar YM, Cannegieter SC, Vonk Noordegraaf A, Delcroix M, Pruszczyk P, Mairuhu ATA, Huisman MV, Klok FA. Incidence of chronic thromboembolic pulmonary hypertension after acute pulmonary embolism: a contemporary view of the published literature. *Eur Respir J*. 2017;49:1601792.
- Delcroix M, Torbicki A, Gopalan D, Sitbon O, Klok FA, Lang I, Jenkins D, Kim NH, Humbert M, Jais X, Noordegraaf AV, Pepke-Zaba J, Brénot P, Dorfmueller P, Fadel E, Ghofrani HA, Hoepfer MH, Jansa P, Madani M, Matsubara H, Ogo T, Grünig E, D'Armini A, Galie N, Meyer B, Corkery P, Meszaros G, Mayer E, Simonneau G. ERS statement on chronic thromboembolic pulmonary hypertension. *Eur Respir J*. 2020;57(6):2002828.
- Huisman MV, Barco S, Cannegieter SC, Le Gal G, Konstantinides SV, Reitsma PH, Rodger M, Noordegraaf AV, Klok FA. Pulmonary embolism. *Nat Rev Dis Primers*. 2018;4:18028.
- Pepke-Zaba J, Delcroix M, Lang I, Mayer E, Jansa P, Ambroz D, Treacy C, D'Armini AM, Morsolini M, Snijder R, Bresser P, Torbicki A, Kristensen B, Lewczuk J, Simkova I, Barberà JA, de Perrot M, Hoepfer MM, Gaine S, Speich R, Gomez-Sanchez MA, Kovacs G, Hamid AM, Jais X, Simonneau G. Chronic thromboembolic pulmonary hypertension (CTEPH): results from an international prospective registry. *Circulation*. 2011;124:1973–81.
- Delcroix M, Lang I, Pepke-Zaba J, Jansa P, D'Armini AM, Snijder R, Bresser P, Torbicki A, Mellekjaer S, Lewczuk J, Simkova I, Barberà JA, de Perrot M, Hoepfer MM, Gaine S, Speich R, Gomez-Sanchez MA, Kovacs G, Jais X, Ambroz D, Treacy C, Morsolini M, Jenkins D, Lindner J, Darteville P, Mayer E, Simonneau G. Long-term outcome of patients with chronic thromboembolic pulmonary hypertension: results from an international prospective registry. *Circulation*. 2016;133:859–71.
- Ende-Verhaar YM, van den Hout WB, Bogaard HJ, Meijboom LJ, Huisman MV, Symersky P, Vonk-Noordegraaf A, Klok FA. Healthcare utilization in chronic thromboembolic pulmonary hypertension after acute pulmonary embolism. *J Thromb Haemostasis*. 2018;16:2168–74.
- Klok FA, Barco S, Konstantinides SV, Darteville P, Fadel E, Jenkins D, Kim NH, Madani M, Matsubara H, Mayer E, Pepke-Zaba J, Delcroix M, Lang IM. Determinants of diagnostic delay in chronic thromboembolic pulmonary hypertension: results from the European CTEPH Registry. *Eur Respir J*. 2018;52:1801687.
- Klok FA, Couturaud F, Delcroix M, Humbert M. Diagnosis of chronic thromboembolic pulmonary hypertension after acute pulmonary embolism. *Eur Respir J*. 2020;55:2000189.
- Guérin L, Couturaud F, Parent F, Revel MP, Gillaizeau F, Planquette B, Pontal D, Guégan M, Simonneau G, Meyer G, Sanchez O. Prevalence of chronic thromboembolic pulmonary hypertension after acute pulmonary embolism. Prevalence of CTEPH after pulmonary embolism. *Thromb Haemostasis*. 2014;112:598–605.
- Ende-Verhaar YM, Meijboom LJ, Kroft LJM, Beenen LFM, Boon GJAM, Middeldorp S, Nossent EJ, Symersky P, Huisman MV, Bogaard HJ, Vonk Noordegraaf A, Klok FA. Usefulness of standard computed tomography pulmonary angiography performed for acute pulmonary embolism for identification of chronic thromboembolic pulmonary hypertension: results of the InShape III study. *J Heart Lung Transplant*. 2019;38:731–38.
- Boon G, Ende-Verhaar YM, Beenen LFM, Coolen J, Delcroix M, Golebiowski M, Huisman MV, Mairuhu ATA, Meijboom LJ, Middeldorp S, Pruszczyk P, van Rooden CJ, Vonk Noordegraaf A, Kroft LJM, Klok FA. Prediction of chronic thromboembolic pulmonary hypertension with standardised evaluation of initial computed tomography pulmonary angiography performed for suspected acute pulmonary embolism. *Eur Radiol*. 2021;32(4):2178–87.
- Braams NJ, Boon G, de Man FS, van Es EJ, den Exter PL, Kroft LJM, Beenen LFM, Huisman MV, Nossent EJ, Boonstra A, Vonk Noordegraaf A, Ruigrok D, Klok FA, Bogaard HJ, Meijboom LJ. Evolution of CT findings after anticoagulant treatment for acute pulmonary embolism in patients with and without an ultimate diagnosis of CTEPH. *Eur Respir J*. 2021;58(6):2100699.
- Boon GJAM, Jairam PM, Groot GMC, van Rooden CJ, Ende-Verhaar YM, Beenen LFM, Kroft LJM, Bogaard HJ, Huisman MV, Symersky P, Vonk Noordegraaf A, Meijboom LJ, Klok FA. Identification of chronic thromboembolic pulmonary hypertension on CTPAs performed for diagnosing acute pulmonary embolism depending on level of expertise. *Eur J Intern Med*. 2021;93:64–70.

15. Rogberg AN, Gopalan D, Westerlund E, Lindholm P. Do radiologists detect chronic thromboembolic disease on computed tomography? *Acta Radiol.* 2019;60:1576–83.
16. Boon GJAM, Ende-Verhaar YM, Bavalia R, El Bouazzaoui LH, Delcroix M, Dzikowska-Diduch O, Huisman MV, Kurnicka K, Mairuhu ATA, Middeldorp S, Pruszczyk P, Ruigrok D, Verhamme P, Vliegen HW, Vonk Noordegraaf A, Vriend JWI, Klok FA. Non-invasive early exclusion of chronic thromboembolic pulmonary hypertension after acute pulmonary embolism: the InShape II study. *Thorax.* 2021;76:1002–09.
17. Klok FA, Van Der Bijl N, Eikenboom HCJ, Van Rooden CJ, Ds Roos A, Kroft LJM, Huisman MV. Comparison of CT assessed right ventricular size and cardiac biomarkers for predicting short-term clinical outcome in normotensive patients suspected of having acute pulmonary embolism. *J Thromb Haemostasis.* 2010;8:853–56.
18. Klok FA, van Kralingen KW, van Dijk APJ, Heyning FH, Vliegen HW, Huisman MV. Prospective cardiopulmonary screening program to detect chronic thromboembolic pulmonary hypertension in patients after acute pulmonary embolism. *Haematologica.* 2010;95:970–75.
19. Klok FA, Zondag W, van Kralingen KW, van Dijk APJ, Tamsma JT, Heyning FH, Vliegen HW, Huisman MV. Patient outcomes after acute pulmonary embolism. A pooled survival analysis of different adverse events. *Am J Respir Crit Care Med.* 2010;181:501–06.
20. van der Bijl N, Klok FA, Huisman MV, van Rooden JK, Mertens BJA, de Roos A, Kroft LJM. Measurement of right and left ventricular function by ECG-synchronized CT scanning in patients with acute pulmonary embolism. *Chest.* 2011;140:1008–15.
21. Zhai Z, Staring M, Hernández Girón I, Veldkamp WJH, Kroft LJ, Ninaber MK, Stoel BC. Automatic quantitative analysis of pulmonary vascular morphology in CT images. *Med Phys.* 2019;46:3985–97.
22. Zhai Z, Staring M, Zhou X, Xie Q, Xiao X, Bakker ME, Kroft LJ, Lelieveldt BPF, Boon GJAM, Klok FA, Stoel BC. Linking Convolutional Neural Networks with Graph Convolutional Networks: Application in Pulmonary Artery-Vein Separation. Cham: Springer International Publishing; 2019. p. 36–43.
23. Stoel BC, Stolk J. Optimization and standardization of lung densitometry in the assessment of pulmonary emphysema. *Invest Radiol.* 2004;39:681–88.
24. Zhai Z, Ota H, Staring M, Stolk J, Sugimura K, Takase K, Stoel BC. Treatment effect of balloon pulmonary angioplasty in chronic thromboembolic pulmonary hypertension quantified by automatic comparative imaging in computed tomography pulmonary angiography. *Invest Radiol.* 2018;53:286–92.
25. Stoel BC, Stolk J, Bakker ME, Parr DG. Regional lung densities in alpha-1 antitrypsin deficiency compared to predicted values. *Respir Res.* 2019;20:45.
26. Zhai Z, Staring M, Ninaber MK, Vries-Bouwstra JK, Schouffoer AA, Kroft LJ, Stolk J, Stoel BC. Pulmonary vascular morphology associated with gas exchange in systemic sclerosis without lung fibrosis. *J Thorac Imaging.* 2019;34:373–79.
27. Rahaghi FN, Ross JC, Agarwal M, González G, Come CE, Diaz AA, Vegas-Sánchez-Ferrero G, Hunsaker A, Estépar RSJ, Waxman AB, Washko GR. Pulmonary vascular morphology as an imaging biomarker in chronic thromboembolic pulmonary hypertension. *Pulm Circ.* 2016;6:70–81.

How to cite this article: Zhai Z, Boon GJAM, Staring M, Dam LF, Kroft LJM, Hernández Girón I, Ninaber MK, Bogaard HJ, Meijboom LJ, Vonk Noordegraaf A, Huisman MV, Klok FA, Stoel BC. Automated quantification of the pulmonary vasculature in pulmonary embolism and chronic thromboembolic pulmonary hypertension. *Pulm Circ.* 2023;13:e12223.

<https://doi.org/10.1002/pul2.12223>